Thermochromic Properties of Some Colored Oxide Materials

Gabriel Ferro, Davy Carole, François Cauwet, Loren Acher, Hyewon Ji, Rodica Chiriac, François Toche, Arnaud Brioude

Thermochromic properties of some colored oxide materials

Gabriel FERRO[1], Davy CAROLE[1], François CAUWET[1], Loren ACHER[1], Hyewon JI[1], Rodica CHIRIAC[1], François TOCHE[1], Arnaud BRIOUDE[1]

[1]Laboratoire Multimatériaux et Interfaces, UMR CNRS 5615, Université Claude Bernard Lyon 1, France

Abstract

The thermochromic properties up to 500°C of some colored, commercial and non-toxic oxides were studied. It includes Bi_2O_3, Fe_2O_3, In_2O_3, WO_3, Er_2O_3, YAG:Ce (Ce doped yttrium aluminum garnet $Y_3Al_5O_{12}$) and YInMn-Blue (Mn doped yttrium indium oxide $YInO_3$). From the CIELAB colorimetric parameters (L*a*b*), evolution of the color contrast ΔE with temperature was calculated. It allowed estimating that most of these oxides change color reversibly with increasing temperature. Two exceptions were identified: i) Er_2O_3 which stayed almost identically pink on all the temperature range and ii) WO_3 which original color was not recovered upon cooling back to room temperature. While the color change of the other oxides was gradual with increasing temperature, YAG:Ce compound behaved differently since its thermochromicity abruptly started above 300°C. The obtained datasets for all these compounds can be used for anticipating the thermochromic properties of these powders and the blends made out of them.

Introduction

Reversible thermochromic materials share the property of changing color reversibly upon temperature variation, i.e. colored is restored upon coming back to the original temperature [1]. Several potential applications have been reported depending on the temperature range of interest: below 100°C for smart windows [2], clothing [3] or ink [4] and at higher temperatures for safety sensors or warning signals or simply temperature indicators [5]. For the high temperature applications, the thermochromic materials need to withstand the temperature change under air so that they should be thermally and chemically stable, in addition to be composed of non-toxic elements. The studied compounds are thus almost exclusively metal oxides. Their color change with temperature is usually not abrupt and rather moderate so that research focuses on complex and/or new oxides for trying to improve the color contrast, such as with pure or doped $Y_3Fe_5O_{12}$ [6], $Er_3Ga_5O_{12}$ [7], $(Bi_{1-x}Y_x)_2O_3$ [8], $Ca_{14}Zn_6Ga_{10}O_{35}$ [9], $SrZr_4(PO_4)_6$ [10] or $Sm_{3-x}Bi_xFe_5O_{12}$ [11].

But, do we really know the thermochromic properties of all the commercially available non-toxic colored oxides? For sure not. Some of them are known to be thermochromic (e.g. Bi_2O_3

[12,13], Fe_2O_3 [5] or WO_3 [14]) but detailed reports on their color change (showing photos and with CIE-Lab parameters) over a large temperature range can hardly be found. Some other commercial colored oxides have not been studied yet for their thermochromic properties. The goal of the present work is to fill the gap by characterizing the thermochromic properties up to 500°C of some commercially available colored oxides for sake of data-set completion. These data could be useful for anticipating the thermochromic properties of blends made out of these oxides as well as for identifying thermostable pigments (which do not change color with temperature) among them.

Experimental

The colored oxides studied in this work are commercially available powders displaying a certain color at room temperature (see Table 1 for more information on these powders). A homemade set-up was used for both qualitative and quantitative color estimation in combination with heating (see figure 1). It is composed of a heating stage (thermocouple-controlled) positioned inside a closed box and uniformly illuminated from the top using commercial white light-emitting diodes (light temperature ~5900 K). This is pretty close to the CIELAB standard D65 illuminant used in L*a*b* measurements for the simulation of daylight. An external camera can take pictures of the samples by uncovering the central hole on the top side. The powders were placed on a dull-white boron nitride (BN) holder having shallow circular prints of 2 mm depth and 1 cm diameter. Each print was fully filled with a single powder and gently pressed in order to display an averagely flat and homogeneous surface. The BN holder was then placed on the heating stage before starting the heating procedure. Note that the use of a BN holder ensures good thermal conduction while avoiding both chemical reactivity with the metallic heating stage and metallic reflection of the light from the stage which could induce color estimation errors. Outside but close to the heating stage are placed a $BaSO_4$ pellet and a graphite powder respectively for fixing the white and black levels of the images. The heating procedure consisted in the succession of controlled heating ramps (5°C/min for 5 min) followed by temperature plateaux (3 min duration) every 25°C from room temperature to 500°C. Each picture was taken after 2 min of temperature stabilization for each plateau. A picture was also taken after cooling back to RT for reversibility check. After adjusting the color tunes using the white and black references, the CIE-Lab colorimetric parameters (L*a*b*) of the different powders were then extracted from these images using GIMP software considering an average area of 20x20 pixels. Color contrast versus temperature (ΔE) was determined using the following formula:

$$\Delta E = \sqrt{(L_T^* - L_{RT}^*)^2 + (a_T^* - a_{RT}^*)^2 + (b_T^* - b_{RT}^*)^2} \qquad \text{Eq (1)}$$

with L^*_T, a^*_T and b^*_T the CIE-Lab parameters at the measured temperature T and L^*_{RT}, a^*_{RT} and b^*_{RT} the CIE-Lab parameters at room temperature (RT).

Each powder has been characterized by UV-visible diffuse reflectance spectroscopy at room temperature using a Bruker UV-NIR 1050+ spectrophotometer equipped with an integrating sphere. For some oxides, Kubelka-Munk equation was used to transforms these reflectance spectra in absorption data in order to determine the band gap using the so-called Tauc plot. Some powders were additionally characterized by differential scanning calorimetry (DSC) with the DSC1 apparatus from Mettler Toledo in order to check for any physico-chemical event which could occur within the temperature range studied. Samples were analysed in 40 µL aluminium crucible, from room temperature up to 500°C, under air and with a rate of 10 $K.min^{-1}$. Prior to analyses, the DSC was calibrated in terms of melting temperature and enthalpy with pure In and Zinc. The relative errors were below 0.2 and 0.6 % for the melting temperature and enthalpy respectively.

Table 1. List of the commercial oxide powders studied in this work

Material	Color at RT	Grain size	Purity	Supplier
Bi_2O_3	Cream yellow	NS [#]	≥98%	Sigma-aldrich
Fe_2O_3	Dark red	< 5 µm	≥96%	Sigma-aldrich
In_2O_3	Pale yellow	NS [#]	99.5%	Merck
Er_2O_3	Light pink	NS [#]	≥99.99	Aldrich
WO_3	Light green	≤ 25µm	99%	Aldrich
YAG:Ce *	Bright yellow	20-40 µm	99%	Merck
YInMn-Blue **	Deep blue	1.3 µm	NS	Kremer Pigmente

* Ce-doped yttrium-aluminum garnet ($Y_3Al_5O_{12}$) / ** $YIn_{1-x}Mn_xO_3$
[#] NS = not specified

Results

The resulting temperature dependences of the L*, a* and b* parameters for the studied commercial powders are listed in Table 2. From these data, the color contrast ΔE was calculated using Eq. (1) for each compound and at each temperature. The results are plotted in Figure 2. One can see that all oxides display a thermochromic behavior except for Er_2O_3 which color remains almost unaffected by temperature. The maximum color changes (from RT to 500°C) are better seen in Figure 3. Obviously, the thermochromic compounds studied here can be separated into two families: the ones really changing color (Bi_2O_3, WO_3, YAG:Ce and In_2O_3) and the ones simply darkening (Fe_2O_3 and YInMn). The latter family (composed of already rather dark powders at RT (with low L* values) gives smaller values of ΔE but with

almost linear evolutions with temperature, while the former family displays the highest ΔE values associated with apparently more complex temperature dependences.

The values of ΔE at 25°C in Figure 2, referred to as "Back RT, correspond to the color contrasts obtained after coming back to room temperature. They thus allow estimating the contrast possibly induced by the thermal cycling and can be considered as a first check of reversibility. After cycling, one can see that almost all the studied compounds have ΔE values < 3.5 upon coming back to RT which means that the difference is hardly noticed by human eye according to [15]. From our experience, taking into account the measurement errors and any possible thermally induced side-effect, such as residual water/humidity desorption, a ΔE values < 5 after cycling should corresponds to a fully reversible thermochromic material. The only exception among the studied oxides is WO_3 which leads to a ΔE value after cycling as high as ~14. This material does not seem to be reversibly thermochromic. This point will be discussed later. Finally, all the powders were characterized by UV-Vis reflectance spectroscopy at RT. The recorded spectra are shown in Figure 4 and separated in two sets: a) the semiconductors and b) the non-semiconductors. Let us consider now each case separately.

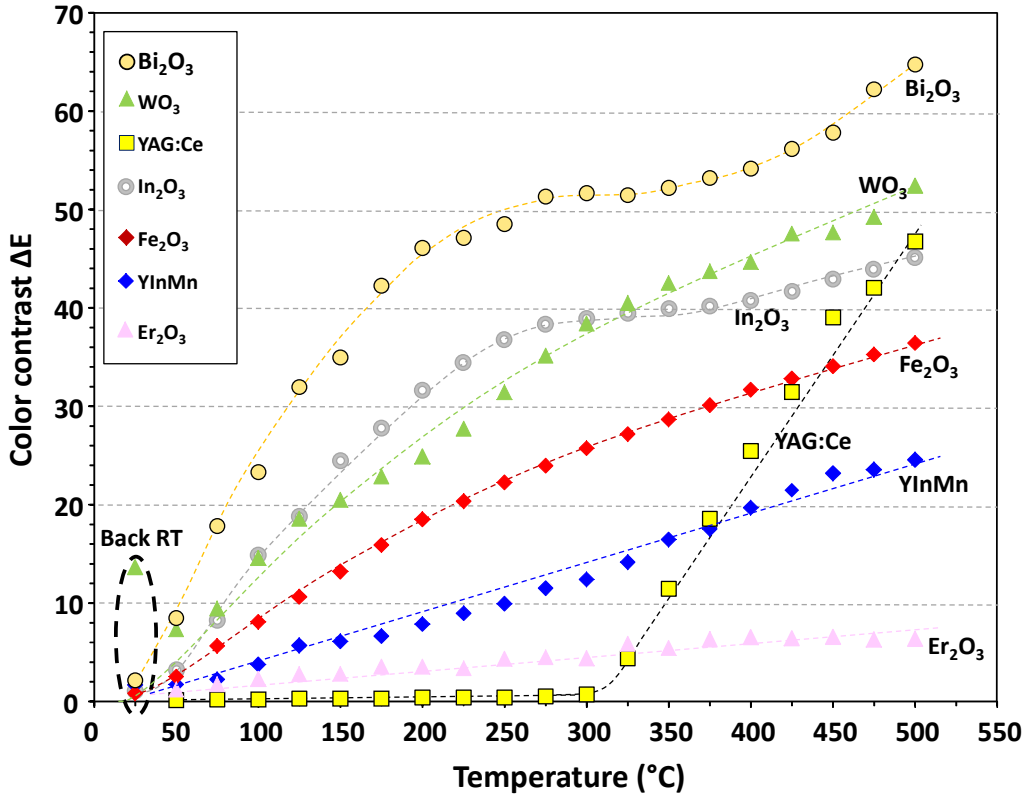

Figure 2. *Temperature dependence of color contrast ΔE for each oxide studied in this work. The points at 25°C correspond to the color contrasts obtained after coming back to room temperature, i.e. contrast induced by the thermal cycling.*

Table 2: Temperature dependence of the L*, a* and b* colorimetric parameters of the commercial colored powders studied in this work

	Bi_2O_3			WO_3			YAG:Ce			In_2O_3			Fe_2O_3			YInMn			Er_2O_3		
	L*	a*	b*	L*	a*	b*	L*	a*	b*	L*	a*	b*	L*	a*	b*	L*	a*	b*	L*	a*	b*
25°C (RT)	92,4	-1,3	30,6	78.7	-10	43.2	97.6	-15.7	93.2	98.4	-8.3	36.1	26	41.2	34.8	15.5	24.5	-54.4	91,8	15	-8,6
50°C	91,3	-3,1	38,8	78.7	-11.4	50.4	97.6	-15.6	93.1	98.2	-8.6	39.4	24.9	39.9	32.9	14.9	23.7	-53	91,2	16	-8,9
75°C	92,6	-3,4	48,3	76.1	-11.7	52.1	97.6	-15.7	93	98	-9.1	44.3	23.1	38.6	30.8	14.9	23.5	-52.5	90,9	16,4	-9,1
100°C	89,3	-1,8	53,7	76.7	-10.9	57.6	97.6	-15.7	93	98.2	-10.8	50.8	22.1	37.3	28.9	13.8	23.2	-51.3	91,2	16,4	-10,3
125°C	90	-2,8	62,4	77.6	-10.9	61.7	97.6	-15.7	92.9	97.8	-11	54.8	21	35.7	27.2	13.4	22.1	-49.7	90,6	17,2	-9,8
150°C	86,3	-0,1	65	77.4	-8.6	63.6	97.6	-15.7	92.9	97.8	-11	54.8	19.9	34.1	25.5	13.6	21.9	-49.2	91,3	16,5	-10,9
175°C	88,9	-2,2	72,7	77.6	-6.7	65.8	97.6	-15.7	92.9	97.6	-12.2	63.6	18.7	32.5	23.7	13.3	21.9	-48.7	90,6	17,5	-10,8
200°C	89,9	-1,2	76,6	77.4	-4.8	67.5	97.5	-15.7	92.8	97.2	-12.1	67.4	17.5	30.9	22	12.5	21.5	-47.8	90,5	17,6	-10,6
225°C	86,6	2,5	77	78.6	-1.6	69.6	97.6	-15.6	92.8	96.9	-12	70.3	16.8	29.7	20.8	12.2	21.1	-46.8	90,6	17,4	-10,6
250°C	87,1	3,3	78,6	80	1	72.6	97.6	-15.7	92.8	96.4	-11.6	72.6	16	28.4	19.6	11.9	20.6	-46	90,2	18,3	-10,9
275°C	87,2	3,7	81,4	81.2	3.6	75.5	97.6	-15.6	92.7	95.4	-10.2	74.3	15.3	27.3	18.5	11.5	19.8	-44.7	90,7	17,7	-12
300°C	84,7	8	80,8	83.1	6.5	77.6	97.5	-15.6	92.5	94.3	-8.5	74.9	14.4	26.1	17.5	11.2	19.3	-44	90,3	18,2	-11,2
325°C	82,2	11	79,5	82.8	9.2	78.6	95.7	-12.5	90.9	92.8	-6	75.1	13.9	25.2	16.5	10.7	18.4	-42.6	90,3	18,7	-12,9
350°C	80,8	15	78,8	82.1	13	78.8	92.5	-6.6	88.5	91.4	-3.4	75.1	13.4	24.3	15.4	10.2	17.1	-40.7	90,4	18,4	-12,6
375°C	78,4	20,6	77	80.8	16.1	78.2	89.3	-0.7	86.1	89.9	-0.8	74.6	12.8	23.3	14.5	10.1	16.5	-39.8	90,3	18,8	-13,4
400°C	74,4	25,3	74,2	79	19.2	77	86.2	5.2	84.2	88,7	1,7	74,4	12.3	22.3	13.4	9.2	15.8	-37.9	89,5	19,8	-12,4
425°C	72,1	29,4	73	76.4	24.6	75.7	83.6	10.3	82.4	87,4	4,3	74,2	11.9	21.4	12.8	8.5	15	-36.5	89,5	19,8	-12,2
450°C	70,2	33,2	71,3	74.6	27.1	72.8	80.4	16.8	80.1	86,1	6,9	73,9	11.6	20.3	12.1	8.7	13.8	-35	90	19,3	-13,2
475°C	65,9	40,3	68,5	71.4	29.6	71.5	79.2	19.4	79.2	84,8	9,4	73,7	11.3	19.2	11.5	8.9	13.8	-34.5	89,8	19,4	-12,6
500°C	62,8	43,7	66,5	68.4	33.9	69.9	77.3	23.6	78.1	83,5	12	73,4	11	18.3	10.8	8.3	13.6	-33.6	89,4	19,8	-12
Back to RT	91.7	-2	32.5	89.3	-10.6	52.6	97.6	-15.6	93.2	98	-8	37	26.1	41.1	34	15.7	23.1	-53.5	91.4	15.2	-9

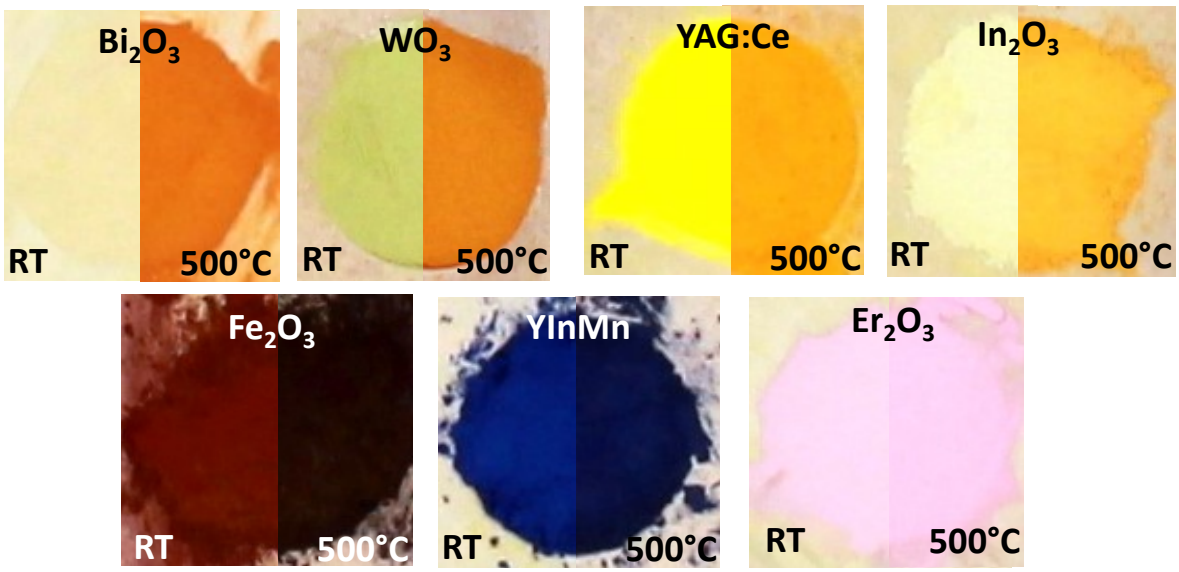

Figure 3. Comparison of the colors obtained at RT and 500°C for each studied oxide.

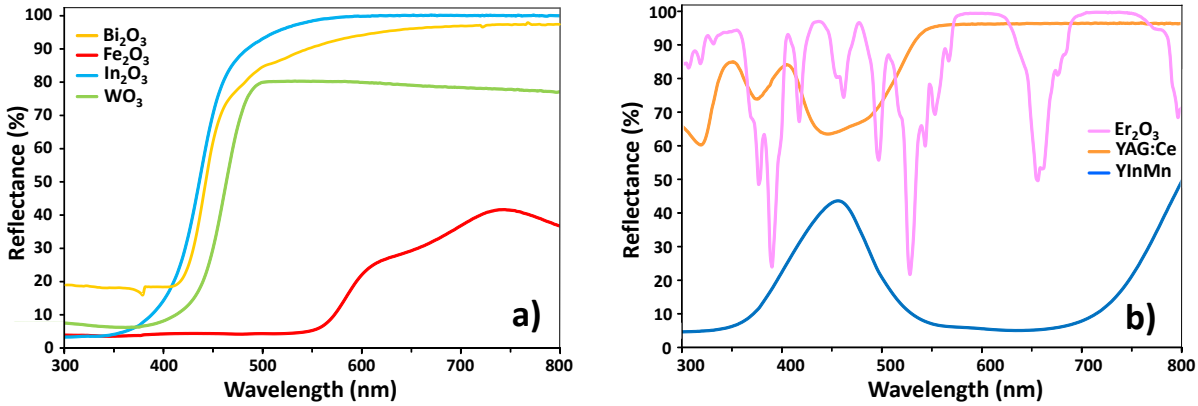

Figure 4. UV-Vis reflectance spectra recorded at RT on a) Bi_2O_3, Fe_2O_3, In_2O_3, WO_3, and b) Er_2O_3, YAG:Ce and YInMn powders.

Bi_2O_3. This oxide displays the highest values of ΔE among the studied compounds, passing from cream yellow at RT to deep orange at 500°C. Bi_2O_3 was already previously identified as thermochromic material [12, 13]. Its ΔE temperature dependence displays an important increase at low temperature (the most important among the studied materials) followed by a plateau at ΔE of ~52 in the temperature range 275-400°C (figure 2). Looking to the effective color of Bi_2O_3 powder at each temperature (figure 5), one cannot see any color stagnation in this specific temperature range. The UV-Vis reflectance spectrum (figure 4a) recorded at RT on Bi_2O_3 powder is typical from a semiconductor material with a unique absorption threshold between 420-450 nm.

In_2O_3. This pale yellow oxide at RT turns to light orange at 500°C and this colour change is fully reversible. Its ΔE temperature dependence has a similar shape as Bi_2O_3 but shifted to lower ΔE value of ~40 (figure 2) despite showing only gradual color evolution in the full temperature range (Figure 5). The corresponding UV-Vis reflectance spectrum (figure 4a) is typical of a semiconductor material with a unique absorption threshold around 450 nm.

WO_3. This compounds passes from light green at RT to deep orange at 500°C. Compared to Bi_2O_3, the perceived color change is also very effective but in different hues, despite smaller ΔE values. ΔE temperature dependence of WO_3 is more regular than for the two previous oxides, i.e. without a plateau (figure 2). Another difference is the moderate reversibility of WO_3 thermochromicity since its ΔE after coming back to RT was calculated as 14, value allowing distinguishing easily the color change by naked eyes. The UV-Vis reflectance spectrum of WO_3 is typical of a semiconductor material with a unique absorption threshold between 450-500 nm (figure 4a).

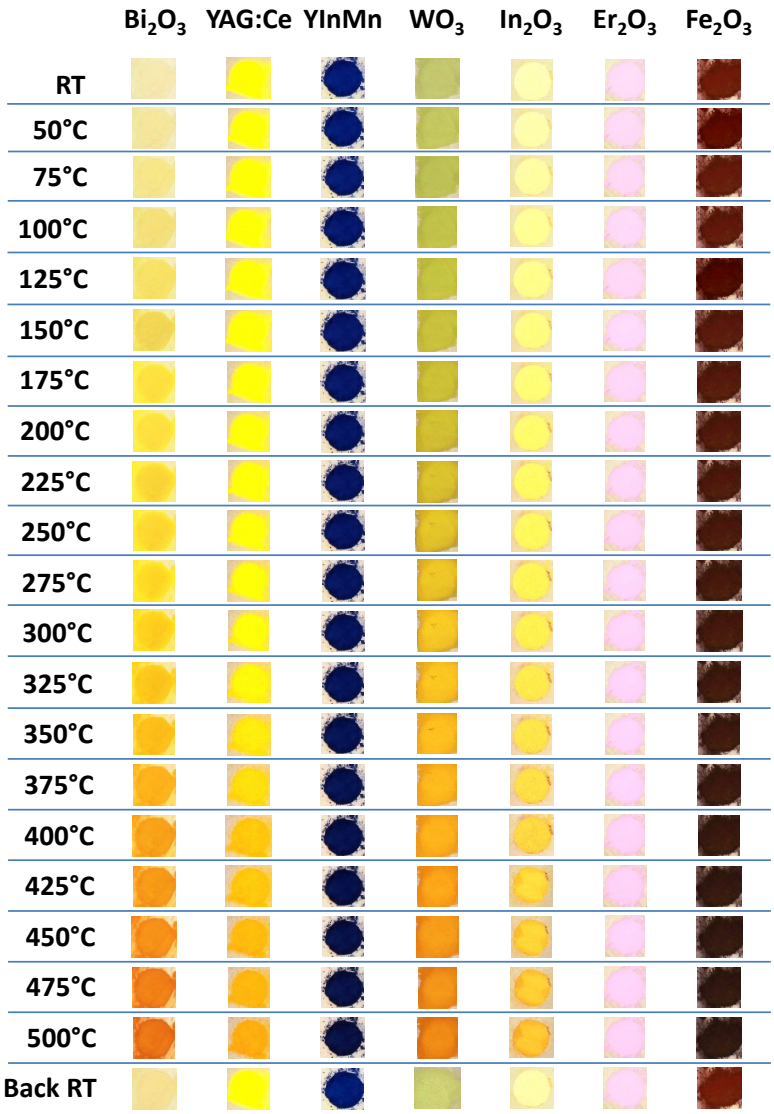

Figure 5. Evolution of the color from RT to 500°C for all the compounds of this study.

YAG:Ce. This bright yellow oxide at RT turns reversibly to bright orange at 500°C. However, its thermochromicity is by far the most uncommon of the series. Indeed, its L*a*b* parameters remain almost constant up to 300°C at which point they start varying (Table 2), generating thus a sudden increase in ΔE (figure 2). The temperature dependence slope above 300°C is the highest in this temperature range, being similar to that of Bi_2O_3 but at lower temperature (< 150°C). From the UV-Vis reflectance spectrum (figure 4b), one can confirm that YAG:Ce is not a semiconductor and that its color is the consequence of its broad absorption band around 450 nm.

Fe_2O_3. This oxide is a well-known dark-red pigment at RT, reversibly passing to almost black–red at 500°C. It is thus a thermochromic material with moderate but almost constant increase of ΔE with increasing temperature. Its thermochromicity mainly consists in continuous darkening of its original color rather than in a real color change. From its UV-Vis reflectance spectrum, one can see that its light absorption is different from other semiconductors of this study. Firstly, its reflectance does not exceed 50% over the entire spectral range (which is to be directly related to its rather dark color). Secondly, its absorption at low energy is not flat and displays large bands.

YInMn. This deep-blue oxide at RT passes reversibly to dark-blue at 500°C. Its temperature dependency of color contrast is rather similar to that of Fe_2O_3 but shifted to lower values (figure 2). Likewise, its thermochromicity mainly consists in continuous darkening of its original color rather than in a real color change (figure 5). From the UV-Vis reflectance spectrum (figure 4b), one can confirm that YInMn is not a semiconductor and that its color is the consequence of its broad absorption band covering the red and yellow spectral region (λ > 500 nm). Note that, like for dark colored Fe_2O_3, its reflectance value does not exceed 50% over the entire visible spectral range.

Er_2O_3. This compound does not really change color with temperature. It simply passes from light pink at RT to slightly deeper pink at 500°C (Figure 3). Its ΔE temperature dependence is as monotonous as for the two previous oxides. But in the case of Er_2O_3, ΔE values remain always < 10 for the entire temperature range while keeping a high color lightness (L* ≥ 89). As a matter of fact, this compound can be considered as a good thermostable pink pigment. From the UV-Vis reflectance spectrum (figure 4b), one can see that Er_2O_3 is not a semiconductor and that its color is the consequence of a complex combination of many narrow absorption bands occurring at various positions of the visible spectral region.

Discussion

The ΔE plateaux observed in Figure 2 for Bi_2O_3 and In_2O_3 are obviously not correlated to the real color evolution since in both cases this evolution is gradual (figure 5). Though no phase transition or other physico-chemical evolution is expected for In_2O_3 in the studied temperature range, this could be different for Bi_2O_3 since several polytypes of this oxide are

known to be stable at RT [16]. XRD analysis of the Bi_2O_3 powder (not shown here) demonstrates that it is of the most stable monoclinic polytype. From DSC analyses, no sharp physico-chemical event has been detected upon heating Bi_2O_3 powder up to 500°C and cooling back to RT (Figure 6). We can thus rule out the possibility of phase transformation for this oxide in the studied temperature range. The expected polytype should be thus the most stable α (monoclinic), as confirmed by its band gap value of 2.86 eV obtained from the Tauc plot shown in figure 7. The band gap values obtained for the other semiconducting oxides (Fe_2O_3, In_2O_3 and WO_3) are in good agreement with the ones reported elsewhere [17-19].

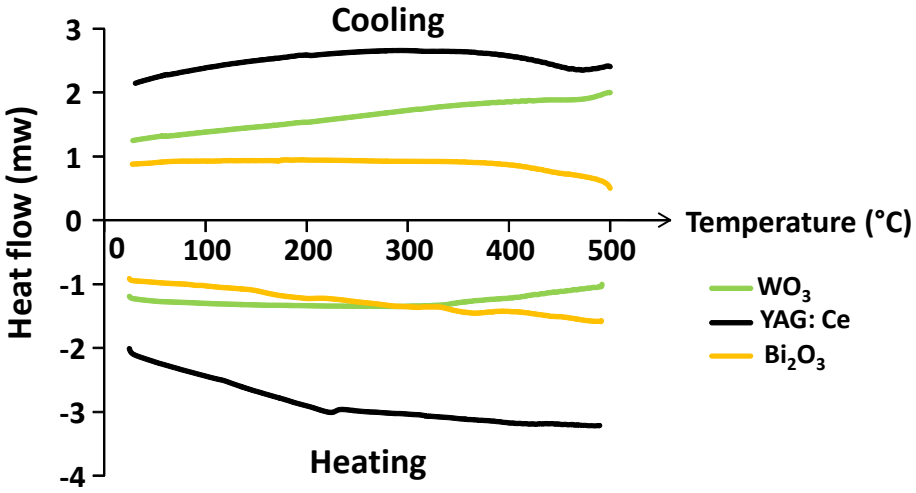

Figure 6. DSC analyses of Bi_2O_3, YAG:Ce and WO_3 powders from RT to 500°C, recorded upon heating and cooling.

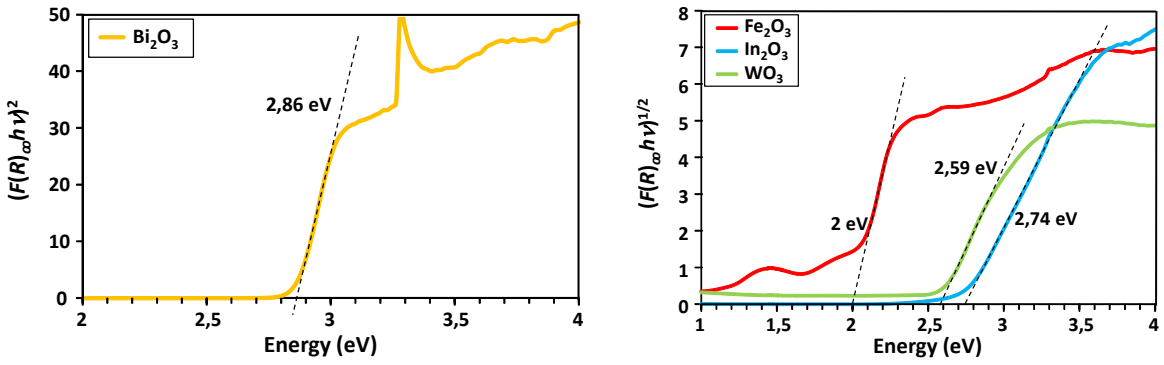

Figure 7. Tauc plots calculated from the reflectance spectra shown in Figure 4a using direct bandgap assumption (n=2) for Bi_2O_3 and indirect one (n=1/2) for Fe_2O_3, In_2O_3 and WO_3. The peak at ~3.3 eV (strong in Bi_2O_3 spectrum but also visible in Fe_2O_3 and WO_3 ones) is a measurement artifact, already visible in Figure 4a, due to the change in source lamp of the spectrometer.

We believe that the plateaux obtained in Figure 2 for Bi_2O_3 and In_2O_3 are due to the ΔE calculations using Eq. 1 which can generate some slope variations in case of uneven evolution of each L*, a* and b* values with temperature. This is illustrated in Figure 8 which plots the generic term from Eq. 1 $(X^*_{(T)} - X^*_{(RT)})^2$ as a function of temperature, with X* corresponding to L*, a* or b* colorimetric parameters for these two oxides. One can see that the effect of b* parameter, which variation is the main one contributing to ΔE at low temperature, saturates then decreases at higher temperature. This is not the case for L* and a* parameters which are rather constant at low temperature while they start increasing rapidly at high temperatures. These dissymmetric evolutions of parameters, when put together in Eq. 1, are thus at the origin of these plateaux.

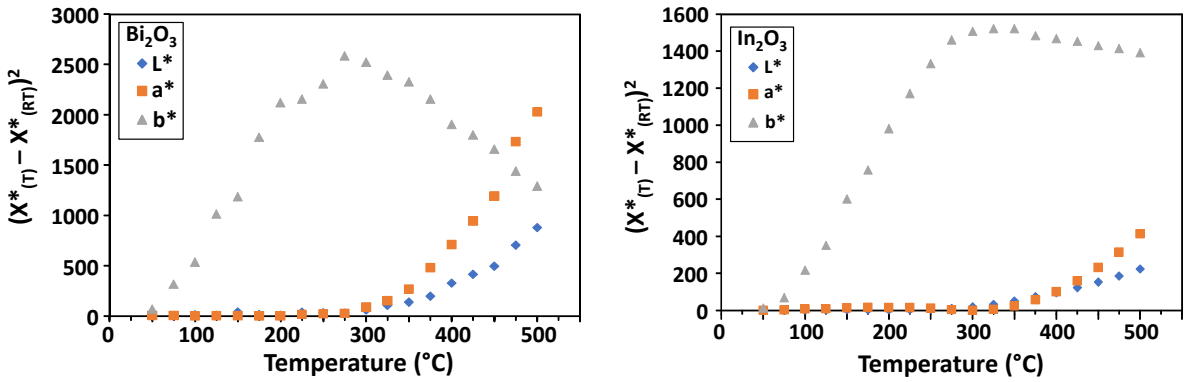

Figure 8. Temperature dependence of each $(X^*_{(T)} - X^*_{(RT)})^2$ subgroup in Eq. 1, with X* = L*, a* or b* colorimetric parameters obtained in this work on Bi_2O_3 (left) and In_2O_3 powders.

Coming now to the case of YAG:Ce powder, its ΔE temperature dependence is peculiar with a sharp increase at ~300°C. However, the DSC analysis (Figure 6) did not show evidence of any phase transition or other physico-chemical event at this temperature that could be expected for such abrupt evolution. Yet, one can notice a little bump at ~230°C associated with a slight change in the slope of the DSC curve upon heating, while nothing is seen upon cooling. A second DSC analysis on the same sample did not display anymore this bump both upon heating and cooling. Finally, using another sample of the same YAG:Ce powder, the bump was again seen by DSC upon heating but disappeared upon cooling. All these results suggest some surface desorption/elimination of volatile species occurring around 230°C. If so, it should not participate to the unusual thermochromic properties found here for YAG:Ce powder, especially when considering that such desorption temperature is a bit far from the expected one for thermochromic transition around 300°C.

Looking closer to the L*a*b* values in Table 2, one can see that in the low temperature range these parameters remain almost constant so that ΔE is almost zero. Observing such an abrupt and reversible thermochromism without clear physico-chemical modification of the material is very uncommon. Usually the colour change is gradual, as can be seen for all the other compounds of this study. However, this YAG:Ce is known to be an efficient yellow

phosphor. This is probably the reason for such a highly bright yellow color at temperatures < 300°C. Above this temperature, it was shown that the luminescence quenches while thermoluminescence appears and gradually increases [20]. This is probably the red-shifting of such thermoluminescence which cause the observed thermochromicity for this material. Note that the thermochromicity of YAG:Ce powder as shown in the present study was never reported before. It should though require deeper investigations for better understanding of the color variation.

Finally, Let us comment the low reversibility observed for WO_3 powder. This compound is known to have different colors, from yellow (stoichiometric), green, blue up to black, depending on its O deficiency (amount of O vacancies) [14,21,22]. XRD analyses performed before and after thermal cycling at 500°C (not shown here) did not evidence any structural change of the powder which remains of the monoclinic polytype. This is confirmed by the DSC analysis which did not detect any phase transition or other physico-chemical event. The color contrast observed for this compound after thermal cycling could thus originate from a variation or deficiency vacancies after heating. One may speculate some photo-thermal assisted reaction with air moisture or with some volatile organic molecules (not detectable by DSC since it operates in darkness), which could have partially reduced the original WO_3 powder.

Conclusion

Among the studied oxides, most of them display reversible color change with increasing temperature up to 500°C. There are two exceptions: i) Er_2O_3 which can be considered as a good thermostable pink pigment and ii) WO_3 which thermal cyclability is questionable. YAG:Ce compound displays the most uncommon thermochromicity since it is observable only above 300°C while for other oxides it is more gradual and starts from RT. The strongest thermochromicity is for Bi_2O_3 powder with ΔE value as high as ~65 at 500°C. The darker powders at RT (YInMn and Fe_2O_3) display the lowest thermochromic properties by simply darkening rather than by true color changing.

References

[1] J.H. Day, *Thermochromism of inorganic compounds*, Chemical Reviews 68 (6) (1968) 649-657

[2] Y. Cui, Y. Ke, C. Liu, Z. Chen, N. Wang, L. Zhang, Y. Zhou, S. Wang, Y. Gao, Y. Long, *Thermochromic VO_2 for Energy-Efficient Smart Windows*; Joule 2, (2018) 1707–1746 / doi: 10.1016/j.joule.2018.06.018

[3] H. Ramlow, K. L. Andrade, A. P. S. Immich, *Smart textiles: an overview of recent progress on chromic textiles*, Journal of the Textile Institute 112(1) (2021) 152-171

[4] R. Kulcar, M. Friskovec, N. Hauptman, A. Vesel, M. K. Gunde, *Colorimetric properties of reversible thermochromic printing inks*, Dyes & Pigments 86 (2010) 271-277 / doi: 10.1016/j.dyepig.2010.01.014

[5] http://tefaletvous.tefal.fr/linnovation-par-tefal/thermo-spot_143

[6] H. Serier-Brault, L. Thibault, M. Legrain, P. Deniard, X. Rocquefelte, P. Leone, J.-L. Perillon, S. Le Bris, J. Waku, S. Jobic, *Thermochromism in Yttrium Iron Garnet Compounds*, Inorg. Chem. 53 (23) (2014) 12378–12383 / doi: 10.1021/ic501708b

[7] H. Liu, H. Qi, L. Yuan, B. Wang, C. Hou, S. Feng, *Design Principles for 3d Electron Transfer in a Ga-based Garnet To Enable High Performance Reversible Thermochromic Material Color Maps*, C*hem. Mater.* 31 (3), (2019) 1048–1056 / doi: 10.1021/acs.chemmater.8b04694

[8] Xi Liu, A. Staubitz, T. M. Gesing, *Thermochromic Behavior of Yttrium-Substituted Bismuth Oxides*, ACS Appl. Mater. Interfaces 11 (2019) 33147−33156 / doi: 10.1021/acsami.9b11450

[9] H. Liu, L. Yuan, X. Wu, X. Hou, M. Tang, C. Hou, H. Chen, S. Feng, *Reversible thermochromic property of Cr, Mn, Fe, Co-doped $Ca_{14}Zn_6Ga_{10}O_{35}$*, J. Mater. Chem. C (8) 2020 9615-9624 / doi: 10.1039/d0tc00921k

[10] I. Yanase, K. Oomori, H. Kobayashi, *Substitution effect of V, Ca, and Ba on the thermochromic properties and thermal expansion of $SrZr_4(PO_4)_6$*, Ceramics International 45 (2019) 5001–5007 / doi: 10.1016/j.ceramint.2018.11.200

[11] H. Liu, L. Yuan, H. Qi, Y. Du, Y. Zhang, C. Hou, S. Feng, *In-situ optical and structural insight of reversible thermochromic materials of $Sm_{3-x}Bi_xFe_5O_{12}$ (x = 0, 0.1, 0.3, 0.5)*, Dyes & Pigments 145 (2017) 418-426 / doi: 10.1016/j.dyepig.2017.06.038

[12] M. Gaudon, P. Deniard, L. Voisin, G. Lacombe, F. Darnat, A. Demourgues, J.-L. Perillon, S. Jobic, *How to mimic the thermo-induced red to green transition of ruby with control of the temperature via the use of an inorganic materials blend?,* Dyes and Pigments 95 (2012) 344-350 / doi: 10.1016/j.dyepig.2012.04.017

[13] A.V. Belykh, A.M. Efremov, M.D. Mikhailov, *Thermochromic material*, patent n° WO 2002/092721 (2004).

[14] M. Weil, W.D. Schubert, *The beautiful colours of tungsten oxides*, Tungsten newsletter june 2013, 1-12

[15] W. Mokrzycki, M. Tatol, *Color difference Delta E - A survey*. Mach. Graph. & Vis. 20 (4) (2011) 383–411.

[16] M. Drache, P. Roussel, J.-P. Wignacourt, *Structures and oxide mobility in Bi-Ln-O materials: heritage of Bi_2O_3*, Chem. Rev. 107 (2007) 80-96 / doi : 10.1021/cr050977s

[17] J.Y. Zheng, Z. Haider, T.K. Van, A.U. Pawar, M.J. Kang, C.W. Kim, Y.S. Kang, *Tuning of the crystal engineering and photoelectrochemical properties of crystalline tungsten oxide for optoelectronic device applications*, Cryst. Eng. Comm. 17 (2015) 6070-6093 / doi: 10.1039/C5CE00900F

[18] G. Ren, Y. Sun, M. Sun, Y. Li, A. Lu, H. Ding, *Visible light enhanced extracellular electron transfer between a hematite photoanode and pseudomonas aeruginosa*, Minerals 7 (2017) 230; doi: 10.3390/min7120230

[19] A. Walsh, J.L.F. Da Silva, S.-H. Wei, C. Körber, A. Klein, L.F.J. Piper, Al. DeMasi, K. E. Smith, G. Panaccione, P. Torelli, D.J. Payne, A. Bourlange, R. G. Egdell, *Nature of the band gap of In_2O_3 revealed by first-principles calculations and x-ray spectroscopy*, Phys; Rev. Lett. 100 (2008) 167402 / doi: 10.1103/PhysRevLett.100.167402

[20] J. Ueda, P. Dorenbos, A.J.J. Bos, A. Meijerink, S. Tanabe, *Insight into the thermal quenching mechanism for $Y_3Al_5O_{12}:Ce^{3+}$ through thermoluminescence excitation spectroscopy*, J. Phys. Chem. C 119 (2015) 25003−25008

[21] S. Chen, Y. Xiao, W. Xie, Y. Wang, Z. Hu, W. Zhang, H. Zhao, Facile strategy for synthesizing non-stoichiometric monoclinic structured tungsten trioxide (WO_{3-x}) with plasma resonance absorption and enhanced photocatalytic activity, Nanomaterials 8 (2018) 553 / doi: 10.3390/nano8070553

[22] Q. Liu, F. Wang, H. Lin, Y. Xie, N. Tong, J. J. Lin, X. Zhang, Z. Zhang, X. wang, *Surface oxygen vacancy and defect engineering of WO_3 for improved visible light photocatalytic performance*, Catal. Sci. Technol. 8 (2018) 4399-4406 / doi: 10.1039/C8CY00994E